Climate Dynamics (2004) 22: 639–651
DOI 10.1007/s00382-004-0412-2

S. J. Kim

The effect of atmospheric CO_2 and ice sheet topography on LGM climate

Received: 8 May 2003 / Accepted: 22 January 2004 / Published online: 5 May 2004

Abstract The role of reduced atmospheric CO_2 concentration and ice sheet topography plus its associated land albedo on the LGM climate is investigated using a coupled atmosphere-ocean-sea ice climate system model. The surface cooling induced by the reduced CO_2 concentration is larger than that by the ice sheet topography plus other factors by about 30% for the surface air temperature and by about 100% for the sea surface temperature. A large inter-hemispheric asymmetry in surface cooling with a larger cooling in the Northern Hemisphere is found for both cases. This asymmetric inter-hemispheric temperature response is consistent in the ice sheet topography case with earlier studies using an atmospheric model coupled with a mixed-layer ocean representation, but contrasts with these results in the reduced CO_2 case. The incorporation of ocean dynamics presumably leads to a larger snow and sea ice feedback as a result of the reduction in northward ocean heat transport, mainly as a consequence of the decrease in the North Atlantic overturning circulation by the substantial freshening of the North Atlantic convection regions. A reversed case is found in the Southern Ocean. Overall, the reduction in atmospheric CO_2 concentration accounts for about 60% of the total LGM climate change.

1 Introduction

Variation in the Earth's orbital parameters has been proposed as the "pacemaker of the ice ages" (Milankovitch 1941; Hays et al. 1976) and this speculation has been supported by spectral analyses of deep-sea sediment cores (e.g., Imbrie et al. 1984) and ice cores (Genthon et al. 1987; Jouzel et al. 1987). Although a change in the seasonal distribution of radiation induced by orbital parameters is believed to initiate the glaciation, the orbital parameters at the Last Glacial Maximum (LGM at about 21 kaBP) are not that different from present-day and cannot directly explain much of the LGM climate (e.g., Hewitt and Mitchell 1997; Broccoli 2000). For the maintenance of the LGM cooling, other physical factors must have been involved.

One of the most important climate forcing components responsible for the LGM cooling is the reduced atmospheric CO_2 concentration. From a chemical analysis of air bubbles trapped in Antarctic ice cores (e.g., Neftel et al. 1982; Barnola et al. 1987), the atmospheric concentration has been estimated as about 200 ppm during the LGM. This is about 80 ppm lower than the pre-industrial CO_2 concentration. Many theories have been suggested to explain this ice-age CO_2 change (see Broecker and Henderson 1998 for review), but there is no consensus on the cause. Nevertheless, a general agreement is that the fluctuations of atmospheric CO_2 concentration are influenced by and influence global climate change.

Another important factor is the expanded continental ice, which influenced and maintained the LGM climate by its height and albedo feedback. CLIMAP (1976, 1981) compiled glacier data and provided the global ice sheet topography of the LGM. More recently Peltier (1994) has published a detailed reconstruction based on the physics of isostatic rebound. According to these reconstructions, a large portion of North America and northern Eurasia was covered by ice sheets (in some places more than 2500 m thick) during the LGM. This volume of the ice sheet requires an estimated LGM sea level drop of about 120 m (e.g., Fairbanks 1989) and the exposed land areas additionally increase the surface albedo.

Other factors playing a role in LGM climate include changes in vegetation and soil type. Numerical model simulations show that the change in surface types could play an important role in LGM climate, especially for

S. J. Kim
Korea Polar Research Institute, KORDI, Ansan P.O. Box 29, Seoul 425-600, Korea
E-mail: seongjkim@kordi.re.kr

regional temperature change over land, through its effect on albedo and evapotranspiration (Crowley and Baum 1997; Wyputta and McAvaney 2001).

Geological and geochemical proxy data have been used to provide a broad picture of LGM climate (e.g., CLIMAP 1976, 1981), but these data cannot deconvolve the response due to each forcing component. A numerical model seems to be a feasible tool for this purpose, though to date few simulations have attempted to study the role of each forcing component. Using an atmospheric general circulation model (AGCM) with the CLIMAP (1981) boundary conditions, Hansen et al. (1984) performed a series of sensitivity experiments to find feedback mechanisms for the LGM cooling and concluded that the land and sea-ice albedo feedback process mainly accounted for the cooling. In a different approach using an AGCM coupled to a mixed-layer ocean model, Manabe and Broccoli (1985) investigated the effect of continental ice on LGM climate. They found that an ice sheet lowers the surface temperature, predominantly in the Northern Hemisphere (NH) and has very little influence on the surface temperature change in the Southern Hemisphere (SH). The failure for the NH ice sheet to cool the SH is due to a missing mechanism of inter-hemispheric heat exchange through ocean currents.

Using GFDL AGCM with a mixed-layer ocean model, Broccoli and Manabe (1987 hereafter BM87) found that the expanded continental ice together with reduced CO_2 concentration accounts for more than 90% of global mean LGM cooling. They found that the ice-sheet effect is confined almost exclusively to the NH (consistent with Manabe and Broccoli 1985), while the reduction of CO_2 concentration cools both hemispheres. They attribute the cooling of the SH primarily to the reduction of atmospheric CO_2 concentration. Using the UKMO Hadley Centre AGCM (HADSM2) with a mixed layer ocean model, Hewitt and Mitchell (1997 hereafter HM97) obtained that about two-thirds of the simulated glacial cooling is due to the presence of the ice sheet through its topography and albedo change.

These studies have provided useful information in understanding the role of each forcing component. The models used for these studies, however, do not include a comprehensive representation of the ocean. This clearly does not allow any changes in oceanic dynamics and associated heat transport that could be a significant factor in the SH cooling as pointed out by Manabe and Broccoli (1985). The current study uses a fully coupled climate system model (three dimensional representations of atmospheric and oceanic general circulation), which includes configurations for both dynamic and thermodynamic processes in the ocean as well as coupled ocean-atmosphere processes. The objective of this study is to investigate the effect of the change in the CO_2 concentration and the ice-sheet topography plus the change in other factors on the LGM climate using a fully dynamic ocean model coupled to an AGCM and sea-ice model.

2 Model structure and experiments

The model used in the current study is the second generation Canadian Centre for Climate Modelling and Analysis (CCCma) coupled general circulation model (CGCM2). A detailed description of the atmosphere, ocean, sea ice, and land surface components of CGCM2 is given in other papers (McFarlane et al. 1992; Flato et al. 2000; Kim et al. 2002, 2003 and references therein). A brief summary is provided here.

The atmospheric component of CGCM2 has T32 horizontal resolution, which is 3.75° ×3.75° in Gaussian grids, and 10 vertical levels. The oceanic component is based on the GFDL MOM version 1.1 with a horizontal resolution of 1.875° ×1.875° and 29 vertical layers. The ocean model includes ocean mixing represented by vertical and isopycnal diffusion, along with the eddy stirring parametrization of Gent and McWilliams (1990) (GM). The sea-ice model includes a representation of ice dynamics with the cavitating fluid rheology of Flato and Hibler (1992) and a simple representation of ice thermodynamics from Semtner (1976). The atmosphere and ocean components interact once per day exchanging heat, freshwater, and momentum. Monthly heat and freshwater flux adjustment fields are applied in all experiments.

The results of three experiments are analyzed (Table 1). The control simulation has a specified CO_2 concentration of 330 ppm, and a contemporary land mask and topography (Flato and Boer 2001). The second experiment features a reduced CO_2 concentration of 235 ppm, a value chosen to reproduce the greenhouse gas forcing difference between contemporary and LGM conditions (Barnola et al. 1987). The third experiment is the LGM simulation which includes the reduced CO_2 concentration of 235 ppm, ice-sheet topography using the ICE-4G reconstruction of Peltier (1994), and a modified land mask based on lowering the sea level by 120 m (Fairbanks 1989). The implemented ice-sheet topography and the change in land mask for the LGM are found in Kim et al. (2002). Orbital parameters are unchanged since they are almost the same as the present. Vegetation and soil types are unchanged except over the glaciated points.CO_2

Table 1 Description of experiments and evaluations

Experiment	*Features*
Control	Present topography and CO_2 concentration (330 ppm)
Reduced CO_2	Reduced CO_2 concentration (235 ppm)
LGM	Reduced CO_2 concentration, LGM ice sheet topography, and sea level change
Effect	*Evaluation*
CO_2	Reduced CO_2 minus Control
ICEAN	LGM minus reduced CO_2 (**ice** sheet, **a**lbedo, and **n**onlinearity)

The control and LGM simulations are described in other papers in detail (Kim et al. 2002, 2003) and not repeated here. Instead, this study investigates the impact on the LGM climate of changes in atmospheric CO_2 concentration and changes in the continental ice plus its associated land albedo change due to sea level drop. The effect of reduced CO_2 concentration has been evaluated by the difference between the control and reduced CO_2 experiment and this evaluation is referred to as "CO_2". Due to the heavy computational requirements of the coupled model, the effect of ice-sheet topography has not been evaluated by a separate experiment. Alternatively, the climate change due to the ice-sheet topography and its associated land albedo change has been evaluated by analyzing the difference between the LGM simulation and the simulation with reduced CO_2 concentration. (Note that the orbital parameters and vegetation types are unchanged in the LGM simulation.) Of course, this difference includes a nonlinear effect. Even though a linear additivity assumption of climate response to different forcing mechanisms has been shown to be nearly valid for the case of relatively small climate change such as in global warming studies (e.g., Ramaswamy and Chen 1997; Haywood et al. 1997), it may not be the case for the substantial climate change like the LGM. This evaluation is referred to as "ICEAN" (**ice** sheet topography, land **a**lbedo, plus **n**onlinear effect).

The ocean responds much more slowly than does the atmosphere. To save computing effort, the ocean component of the model is accelerated for the experiments with the reduced CO_2 concentration and the LGM experiment using a periodically synchronous coupling method that is described by Voss and Sausen (1996). The abrupt imposition of a forcing change at the beginning of a simulation leads to a rapid system adjustment and the potential for overshooting is large. Therefore, the system is kept in a fully coupled mode for the first 300 years for the experiment with the reduced CO_2 concentration and 100 years for the LGM simulation and then the ocean acceleration is applied during the remainder of the integration. A more detailed description of the ocean acceleration method is described in Voss and Sausen (1996) and Kim et al. (2003). The simulation with the reduced CO_2 concentration is integrated for 1300 years, while the LGM simulation is integrated for 900 years. Results averaged over the last 50 years are analyzed.

3 Surface temperature response

In this section, the changes in surface air temperature (SAT) and sea surface temperature (SST) induced by the reduced CO_2 concentration and by the ice-sheet topography and its associated land albedo change are presented. In order to examine the response of different kind of models to the reduced CO_2 and the changes in ice-sheet topography, a comparison to other model results is presented.

Table 2 Global- and hemisphere-mean surface temperature change. Units are in °C

	CO_2			ICEAN		
	NH	SH	Global	NH	SH	Global
SAT	–7.7	–4.3	–6.0	–6.4	–2.7	–4.6
SST	–5.0	–3.6	–4.2	–2.5	–1.7	–2.0

Table 2 summarizes the changes in global- and hemisphere-mean SAT and SST. On a global basis, the surface temperature reduction is larger in the CO_2 case than in the ICEAN case by about 30% for SAT and by about 100% for SST. This CGCM2 model response differs from that of BM87 and HM97. BM87 showed that the ice sheet plus land albedo induced cooling is almost the same as for SST or slightly larger for SAT than that due to the CO_2-induced cooling, while in HM97 about two-thirds of the simulated cooling is due to the presence of the ice sheet.

For both the CO_2 and ICEAN cases, surface cooling is substantially larger in the NH than in the SH. This is particularly the case for ICEAN, where the surface cooling is more than twice as large as in the NH. This temperature response is not surprising because the changes in the ice sheets are predominantly found in the NH. The reduced CO_2 concentration also leads to a larger NH surface cooling by about 80% than in the SH. Whereas this response is consistent with HM97 who obtained about 35% larger cooling in the NH, it is in contrast to that of BM87 who obtained a about 30% larger cooling in the SH. The larger NH cooling in response to reduced CO_2 concentration is presumably associated with snow and ice albedo feedback with the incorporation of ocean dynamics. In the surface ocean cooling, the inter-hemispheric asymmetry is slightly larger in the ICEAN case (about 50%) than in the CO_2 case (about 40%), although the magnitude of cooling is overall larger in the CO_2 case.

The latitudinal profiles of the change in zonally averaged annual-mean SAT and SST are displayed in Fig. 1. A marked reduction in SAT is found over much of the NH with maximum cooling poleward of 60°N associated with the change in snow/ice albedo feedback. Around the equator, the zonally averaged cooling due to the reduced CO_2 concentration is larger than that in the ICEAN case. This is due to the tropical cooling associated with the enhanced upwelling and advection by a La Niña-like response as described subsequently. In the southern high latitudes, on the other hand, the ICEAN case leads to a larger cooling, due to the thicker and wider Antarctic continental ice. In CGCM2, both the CO_2 and ICEAN cases lead to a pronounced cooling from 30°N to the pole. In BM87 only the ice sheet induces such a cooling and the cooling due to the reduced CO_2 is larger in the southern high latitudes.

An extreme asymmetry in surface cooling between hemispheres is also evident in the latitudinal distribution

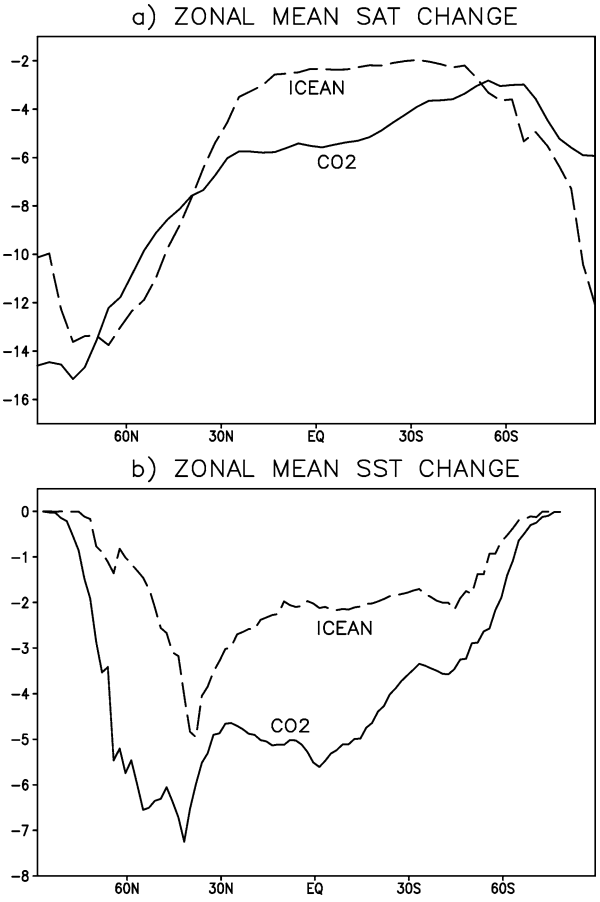

Fig. 1 Latitudinal distribution of the change in annual-mean zonally averaged **a** surface air temperature (SAT) and **b** sea surface temperature (SST) for the CO_2 (*solid*) and ICEAN (*dashed*) cases

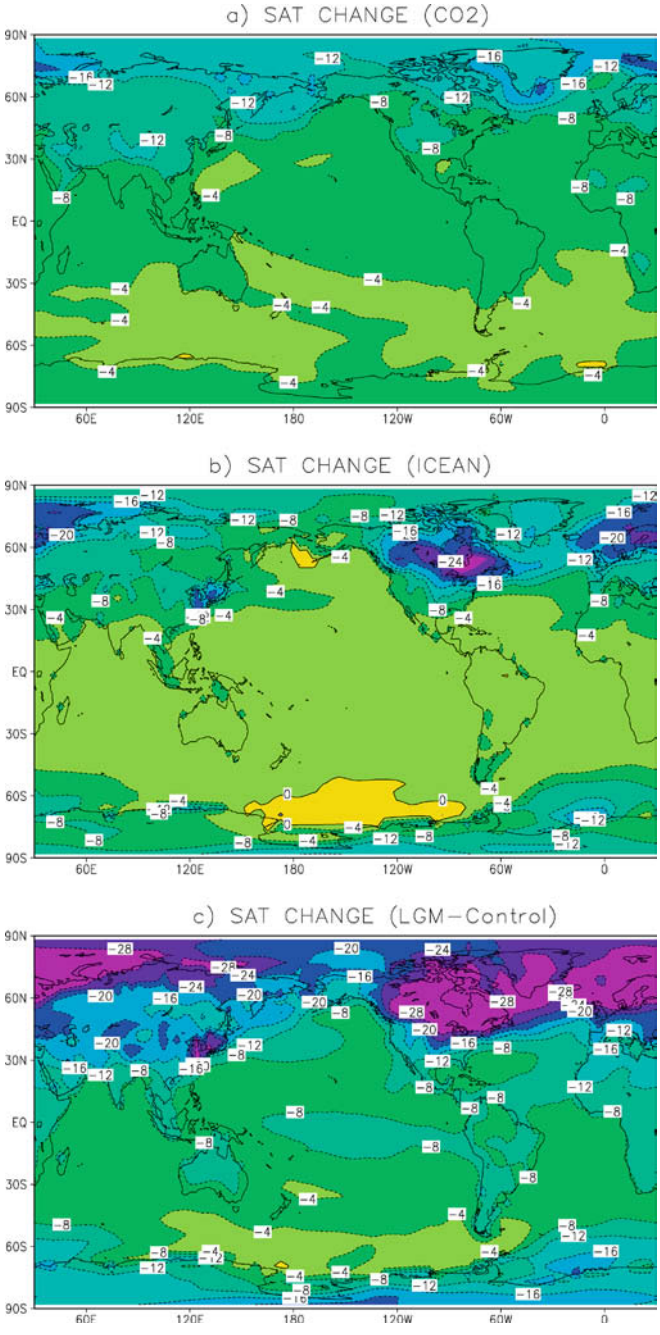

Fig. 2 Geographic distribution of the change in annual-mean SAT for **a** CO_2, **b** ICEAN, and **c** LGM cases. Contour interval is 4 °C

of the change in SST for both cases (Fig. 1b). Maximum SST reduction occurs at about 40°N and these latitudes coincide with locations of enhanced offshore winds. The rate of cooling diminishes toward the equator and the smallest cooling is found at southern high latitudes. The zonally averaged surface ocean cooling due to reduced CO_2 concentration is larger than that due to ice sheets everywhere. This latitudinally asymmetric SST response is in part due to the change in oceanic meridional heat transport as shown in Sect. 5.

Figure 2 displays the geographic distribution of the change in annual-mean SAT. In the CO_2 case, the largest cooling is found over the Arctic, the northern North Atlantic, and the northern North Pacific (Fig. 2a). This is due to the change in sea ice. A marked cooling over Tibet is associated with the change in snow cover. Less cooling is found over the Southern Ocean and this is associated with an increase in the meridional ocean heat transport as illustrated later. The spatial distribution of the change in surface temperature induced by the reduction of CO_2 concentration broadly mirrors the image obtained in a simulation with increased greenhouse gas (Boer et al. 2000). The marked cooling over the Arctic Ocean is a common feature with HM97, while it is not pronounced in BM87. In BM87, the largest cooling is found in the Southern Ocean.

For the ICEAN case, the most apparent change in SAT is the pronounced cooling over North America and northern Europe, reaching more than 20 °C (Fig. 2b). This maximum cooling is due to the ice-sheet elevation, which is more than 2000 m in some regions, and ice-sheet albedo. Another region of notable cooling is the northern North Atlantic where the SAT reduction reaches more than 12 °C, due to the enhanced sea-ice

cover. In the ICEAN case, the degree of cooling is comparatively weaker over the ocean and warming patches are even found in the Pacific sector of the Southern Ocean. The anomalous warming patches are due to less Pacific sea-ice cover in the ICEAN case than the control simulation. The geographic pattern of the SAT response in the ICEAN is on the whole consistent with that obtained in BM87 and HM97, but the degree of cooling is larger in CGCM2, particularly over the ocean.

The surface cooling induced by the LGM forcing change is shown in Fig. 2c. The figure illustrates that the LGM surface cooling is in large part due to the reduced CO_2 concentration, except for North America and northern Europe where the ice-sheet topography plays a predominant role as expected. A large difference in spatial feature of the SAT in comparison to the slab ocean model is found over the ocean associated with the oceanic dynamics response in the coupled model. A more detailed description of the LGM surface cooling is found in another context (Kim et al. 2003)

Figure 3 shows the geographic distribution of the change in SST. The reduced CO_2 concentration produces SST change features found in the CLIMAP reconstructions such as the pronounced cooling over tropical central Pacific (Fig. 3a). This is associated with an enhancement of the equatorial upwelling as a consequence of a La Niña-like response. Other features include cold patches off California and Peru, and elongated cold tongues at the southern tip of Africa and Australia. These are the features produced in a coupled model associated with the role of ocean dynamics but missing in the mixed-layer ocean version of the model as described in Kim et al. (2003).

In the ICEAN case, the most notable feature is the pronounced cooling at northern mid-latitudes (about 40°N) in the Atlantic and Pacific (Fig. 3b). This is the location of strongest offshore winds out of the continent. In comparison to the CO_2 case, the degree of surface ocean cooling is overall lower and the features associated with ocean dynamics are less prominent. This comparison indicates that the reduced CO_2 concentration is mainly responsible for the shaping of the SST change pattern in the LGM climate, as shown in Fig. 3c. In the Arctic Ocean and over the southern margin of the Southern Ocean, the SST change is quite small, whereas the SAT change is substantial in those regions (see Fig. 2c). This difference is due to the thicker sea ice which insulates the atmosphere from surface ocean, while the ocean remains at the freezing temperature.

The surface cooling due to reduced CO_2 concentration is substantially larger in CGCM2 than in BM87 and HM97. This difference is associated with two factors. First, temperature response tends to be larger in a coupled model than that in a mixed-layer ocean model. For example, in response to a doubling of CO_2 the temperature response is about 17% larger in CCCma (Boer and Yu 2003) and 15% in GFDL (Stouffer and Manabe 1999) than in mixed-layer ocean models (Boer et al. 1992; Manabe et al. 1991). Second, model sensitivity tends to be larger by about 50% in colder than in warmer climates (e.g., Manabe et al. 1991; Hansen et al. 1997). This is presumably due to stronger snow and sea-ice feedbacks in colder climate.

Overall, the surface temperature reduction is larger in the CO_2 case than in the ICEAN case and the reduced CO_2 concentration accounts for more than 60% of the total global-mean LGM surface cooling.

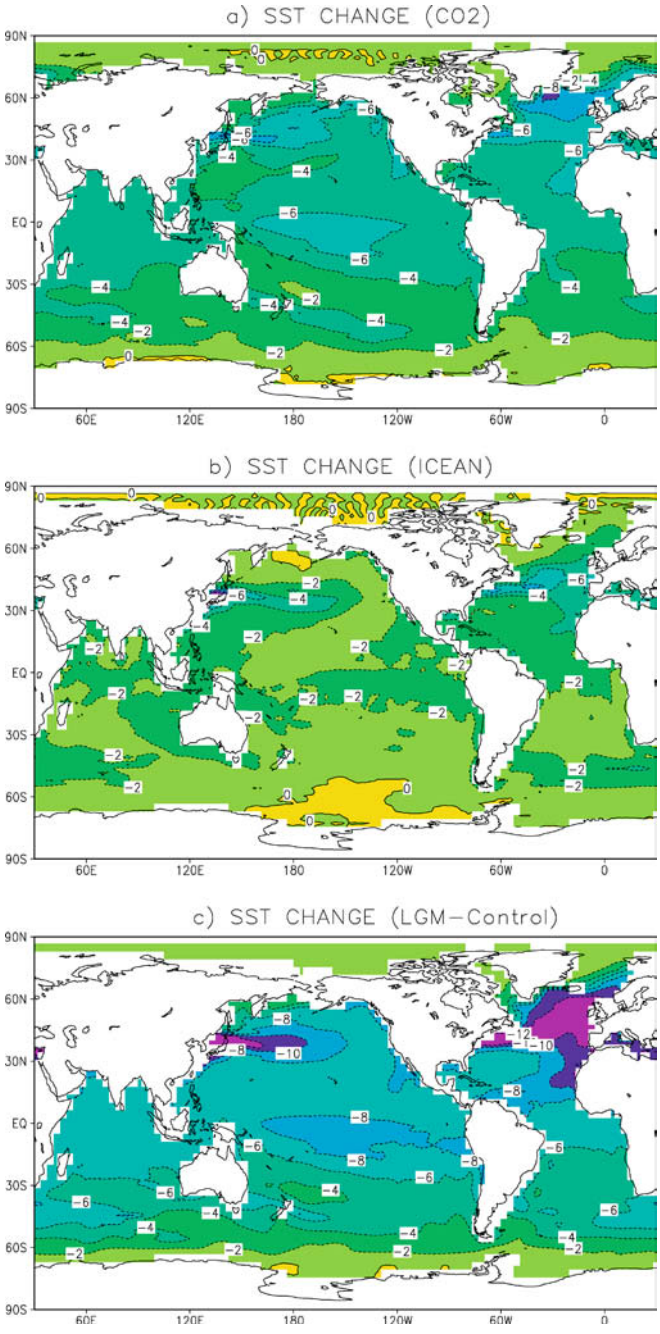

Fig. 3 Geographic distribution of the change in annual-mean SST for **a** CO_2, **b** ICEAN, and **c** LGM cases. Contour interval is 2 °C

4 Surface energy budget

Changes in boundary conditions have a direct impact on the surface energy budget, which consequently modifies the surface temperature. The surface temperature change in turn influences the surface energy budget. This section examines the change in the surface energy budget to the reduced CO_2 concentration and ice-sheet topography plus sea level change.

The surface energy budget is written as, $C^* \frac{\partial T}{\partial t} = (S + F) + (LE + H) + A = R + B + A$, where C^* is the heat capacity of the upper layer, T the surface temperature, S the shortwave and F the longwave radiative heat fluxes, and LE the latent and H the sensible heat fluxes across the surface. R is the net radiative heat fluxes, B the net turbulent heat fluxes, and A represents the effect of vertical and horizontal heat transport. The turbulent heat flux in the model is calculated using the bulk aerodynamic formulae. In quasi-equilibrium, the rate of change term is small and the change in surface heat budget terms is written as $\delta R + \delta B + \delta A = 0$. Note that the sign convention is that all fluxes are positive if they act to warm and negative if they act to cool the layer.

The reduction in CO_2 concentration and the continental ice are expected to result in a net reduction in the radiative heat flux, leading to a surface cooling. The surface cooling consequently acts to reduce the turbulent heat loss and eventually reaches a new surface energy balance. This feature is illustrated in Table 3 which presents the globally and hemispherically averaged values of the difference terms in the surface heat flux. On a global basis, the net reduction in the radiative heat flux is similar for both cases, but for different reasons. In the CO_2 case, the reduction in the radiative heat flux (R) is largely due to the reduction in longwave heat flux (F) because the reduced atmospheric CO_2 concentration directly affects the amount of outgoing longwave radiation. In the ICEAN case, on the other hand, the reduction in R is primarily due to the reduction in the shortwave heat flux (S), because of high ice-sheet albedo. Due to the surface cooling and its associated reduction in evaporation, the change in latent heat flux (LE) acts to warm the surface. Although the sensible heat flux H tends to cool the surface slightly, the latent heat gain is much larger. Eventually, the reduction in radiative heat flux (R) is mostly offset by the increase in net turbulent heat flux (B). The slight mismatches in the net surface energy budget found in both cases are due to an oceanic heat adjustment (A).

Table 3 Global- and hemisphere-mean surface energy budget. Units are in W m^{-2}

	CO_2			ICEAN		
	NH	SH	Global	NH	SH	Global
δR	–7.2	–3.7	–5.5	–8.2	–2.4	–5.3
δS	–2.6	–1.1	–1.9	–6.5	–1.6	–4.1
δF	–4.6	–2.6	–3.6	–1.7	–0.8	–1.2
δB	7.1	0.3	3.7	8.35	1.5	4.9
LδE	9.0	4.0	6.5	8.4	3.5	5.9
δH	–1.9	–3.7	–2.8	–0.05	–2.0	–1.0
δN	–1.3	–3.3	–1.7	0.1	–0.9	–0.4

In CGCM2, the change in radiative heat flux is larger than other model results for both cases. The presence of an ice sheet leads to the reduction of about 1.0 to 2.9 W m^{-2} in other models (BM87; Hoffert and Covey 1992; Hansen et al. 1993; HM97), while in CGCM2 the radiative forcing change in the ICEAN case is –5.3 W m^{-2}. The reduced CO_2 concentration results in the reduction of radiative heat flux by 5.5 W m^{-2} in CGCM2, whereas other models exhibited the change between –1.3 and –1.8 W m^{-2}.

The NH has a much larger (by more than twice) reduction in radiative heat flux than does the SH for both cases. For the ICEAN case, the larger NH reduction in R is primarily due to the reduction in shortwave radiation associated with the ice sheet, whereas in the CO_2 case the larger NH reduction is in large part due to the change in the longwave heat flux (F). The larger NH reduction in R is consistent with BM87 and HM97 for the ICEAN case, but is in contrast for the CO_2 case. In both BM87 and HM97, the decrease in radiative heat flux due to CO_2 reduction is roughly even in both hemispheres.

The interhemispheric asymmetry in the surface energy budget is more clearly illustrated in the changes in zonally averaged shortwave, longwave, turbulent, and net surface heat fluxes given in Fig. 4. Again the positive values represent the heat fluxes such as to warm the surface. For both cases, shortwave heat flux is markedly reduced at mid to high northern latitudes and at around 60°S, while the turbulent heat flux increases substantially in those latitudes. In the low latitudes the short wave heat flux slightly increases for both cases, while the change in the long wave heat flux is such as to cool the surface. In a global warming experiment using a similar version of the atmospheric model, Boer (1993) found a reduced shortwave heat flux at low latitudes. This is a reversed pattern. He attributed the reduced shortwave heat flux to the change in the cloud cover as well as the change in cloud optical properties. The net change in the zonal-mean heat flux is overall small except for the southern high latitudes at about 60°S (Fig. 4d) where there is a noticeable reduction in the net surface heat flux due to oceanic heat adjustment.

Figure 5 displays the geographic distribution of the change in radiative, turbulent, and net heat fluxes. In the CO_2 case, the distinctive reduction in radiative heat flux is found in the northwestern Pacific, northern North Atlantic, and over the Southern Ocean, associated with extended sea-ice cover. A marked reduction in R is also found over the Asian continent, especially around Tibet, associated with the extended snow cover. In the ICEAN case (Fig. 5b), the marked reduction in the radiative heat flux due to continental ice is visible over North America

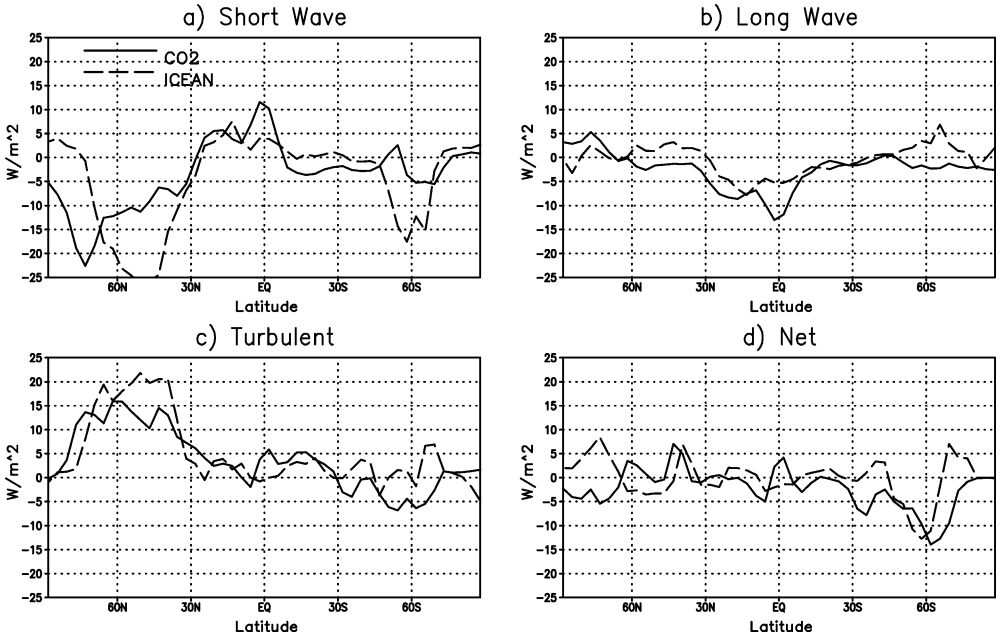

Fig. 4 Zonally averaged annual-mean surface heat flux change for **a** shortwave, **b** longwave, **c** turbulent, and **d** net. Units W m^{-2}

and in northern Europe. Where the radiative heat flux decreases, the change in turbulent heat fluxes act to warm the surface (Fig. 5c, d). Over land the radiative cooling is completely offset by the turbulent heating (Fig. 5e, f). Over ocean, on the other hand, the oceanic heat transport leads to an imbalance in the surface energy budget, in particular, over the Southern Ocean the change in the net surface heat flux is overall negative and in the North Atlantic it is positive for both cases. In other words, the ocean provides heat to the Southern Ocean, while heat is lost in the North Atlantic. This is associated with the change in oceanic meridional heat transport as described in a subsequent section.

To summarize, for both the CO_2 and ICEAN cases, the reduction of the radiative heat flux is much larger in the northern mid to high latitudes primarily due to reduction in the shortwave heat fluxes associated with the snow/ice albedo feedback. At low latitudes, the longwave heat flux is moderately reduced due to the change in the greenhouse effect.

5 Oceanic feedback

5.1 Meridional heat transport

Changes in the ocean heat transport are important in the energy balance and the inter-hemispheric heat exchange via the ocean currents comprises a critical component of the global climate system. The change in the poleward ocean heat transport further modifies the distribution of sea-ice cover and associated albedo feedback.

Figure 6 displays the vertically and zonally integrated heat transport in the global and Atlantic domains for the control simulation (solid), the reduced CO_2 simulation (dashed), and the LGM simulation (dotted). The observationally based estimates of heat transport are rather uncertain. Nevertheless, the simulated heat transport of the control simulation appears to agree reasonably well with observed estimates. For example, on the global domain the maximum northward heat transport simulated in the control simulation is about 1.5 PW (PW = 10^{15} W) at about 15°N and this value is within observed error ranges (see Ganachaud and Wunsch 2000, and references therein). The simulated maximum southward heat transport (about 1.25 PW) is also within the observed error ranges.

On a global domain, the reduced CO_2 concentration results in the decrease of northward heat transport, for example, by about 0.3 PW (20%) at 15°N. The ICEAN leads to the additional reduction of northward heat transport by about 0.2 PW at the same location. In the SH, on the other hand, the southward heat transport is substantially enhanced, for example, by about 0.7 PW (55%) at 15°S. In contrast to the NH, the effect of ICEAN on the southward heat transport is much less than the effect of reduced CO_2 (Fig. 6a).

In the Atlantic domain, the meridional heat transport is northward everywhere in the control simulation. This is due to the northward warm water mass transport in the upper thermocline layer and this feature is supported by the observed estimates (Macdonald and Wunsch 1996; Ganachaud and Wunsch 2000, and references therein). In response to the reduction in CO_2 concentration, a marked reduction in the northward heat transport is found, e.g., by about 50% at about 30°N (Fig. 6b). The ICEAN contributes an additional reduction (by about 15% at 30°N). A more dramatic change is found in the SH where the heat transport direction is reversed for the two cases. For example, for the CO_2 case about 0.3 PW of heat is transported southward at 15°S. This southward transport is further augmented by

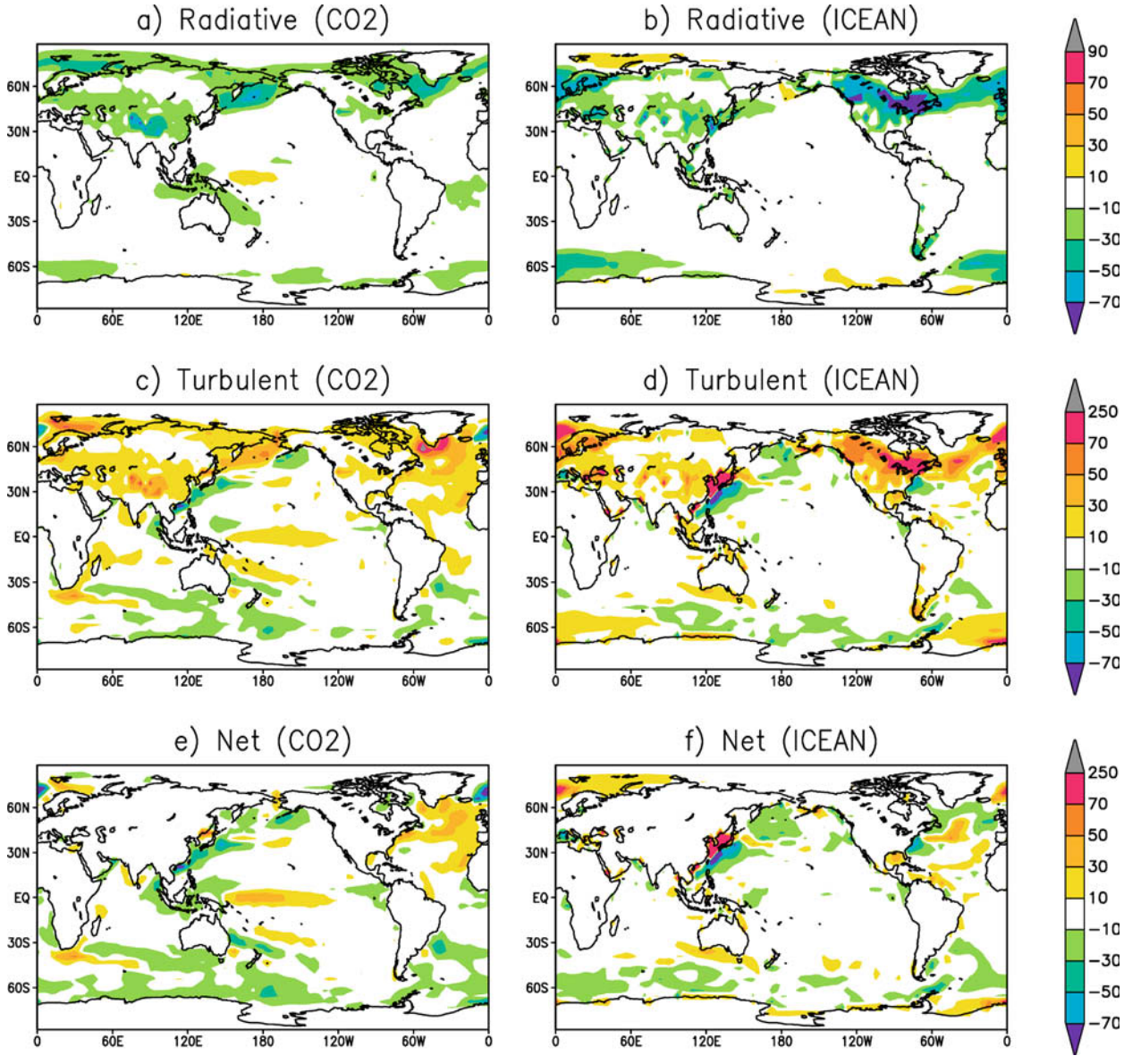

Fig. 5 Geographic distribution of the change in annual-mean surface heat fluxes for **a** radiative, **c** turbulent, **e** net for the CO_2 case and for **b** radiative, **d** turbulent, **f** net for the ICEAN case. Contour interval is 20 W m^{-2}

approximately 0.2 PW (at the same latitude) in the ICEAN case.

The decrease in northward heat flux simulated in CGCM2 agrees with results from studies based on coupled models of intermediate complexity (Weaver et al. 1998; Ganopolski et al. 1998), but contrasts with results obtained by the coupled models of UKMO (Hewitt et al. 2001, 2003), Japan MRI (Kitoh et al. 2001), and NCAR (Shin et al. 2003). These coupled models commonly produced an increase in northward heat transport in LGM simulations. Hewitt et al. (2001, 2003) and Kitoh et al. (2001) attributed the increase in northward heat flux to the enhanced meridional overturning circulation, while Shin et al. (2003) ascribed it to the increase in the Gulf Stream.

Overall, the reduced CO_2 concentration together with ICEAN leads to a marked increase in southward ocean heat transport at the expense of the NH and the SH gains a large amount of heat (e.g. by about 0.5 PW in the Atlantic domain). The modification of the meridional heat transport is primarily due to the change in the oceanic meridional overturning circulation in response to the change in boundary conditions as described in the following section.

5.2 Meridional overturning circulation

The change in meridional heat transport is largely governed by the change in the ocean meridional over-

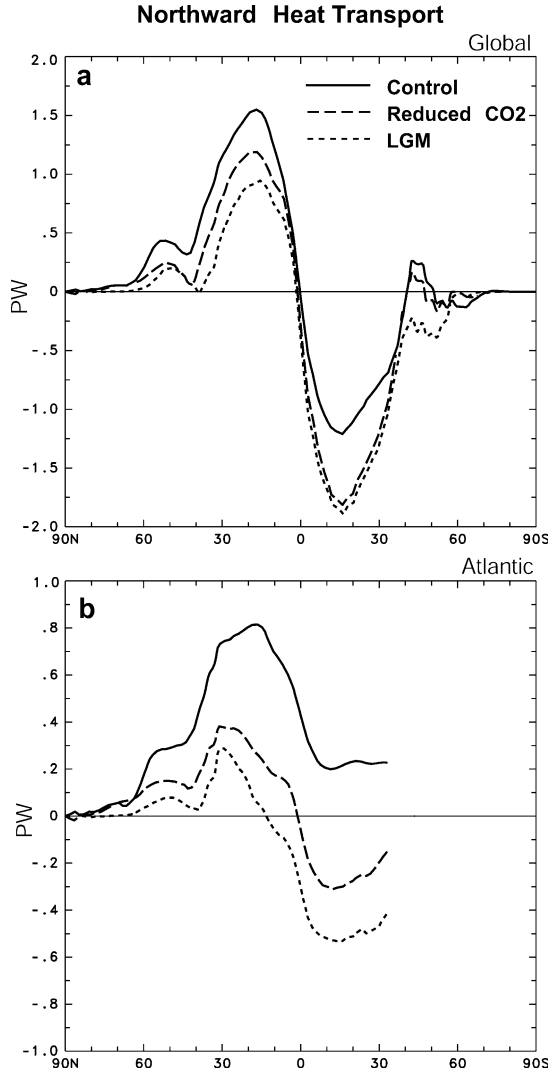

Fig. 6 Zonally integrated annual-mean meridional heat transport for **a** global and **b** Atlantic domains simulated in control (*solid*), reduced CO_2 (*dashed*), and LGM (*dotted*). Units PW (10^{15} W)

turning circulation. Figure 7 displays the meridional overturning stream functions for the control, reduced CO_2 concentration, and LGM simulation in the Atlantic and global domains. In the Atlantic domain, the formation and outflow of North Atlantic Deep Water (NADW) is represented in the large positive overturning cell in the NH. The formation of Antarctic Bottom Water (AABW) is represented as the negative overturning cell near the Antarctic Continent in the global domain (Fig. 7b). The outflow of AABW toward the north is represented as the negative cell in the deep ocean below 3000 m. The strong positive cell at about 60°S, the Deacon cell, is driven by Ekman divergence in response to the westerlies over the Southern Ocean.

In the control simulation, the maximum North Atlantic overturning stream function is about 14 Sv and the AABW outflow is about 4 Sv in the Atlantic domain (Fig. 7a). These values are with in the observed uncertainty ranges. The formation of AABW (about 2 Sv) shown in Fig. 7b is slightly underestimated. A more detailed description for the simulated overturning stream function in the control experiment and comparison to observed estimates is found in Kim et al. (2002).

In the reduced CO_2 simulation, the maximum North Atlantic overturning stream function associated with the NADW formation substantially decreases to 6 Sv (Fig. 7c). This is due to the freshening of the North Atlantic as illustrated in following section. The NADW outflow, which is about 10 Sv at 30°S in the control simulation, also becomes remarkably weaker and is confined to the north of 20°S. On the other hand, the stream function associated with the AABW formation near the Antarctic continent increases substantially to 8 Sv, a fourfold increase (Fig. 7d). The outflow of AABW to the north is enhanced in the deep ocean and the southward return flow is not confined to the deep ocean, but now also found in the upper layer from the equator to 30°S. Note that this return flow is absent in the control simulation due to the predominance of the NADW cell. This enhanced southward return flow in the reduced CO_2 experiment apparently plays a role in strengthening the southward heat transport described in the previous section.

The incorporation of the ice-sheet topography and its associated land albedo change results in a further weakening (by about 2 Sv) of the North Atlantic overturning circulation (Fig. 7e). Additionally, the overturning cell associated with the NADW production is much shallower than that of the control simulation and its outflow is confined to the north of 30°N. The stream function associated with the AABW formation is enhanced to more than 16 Sv (about twice the reduced CO_2 simulation). The AABW outflow in the deep ocean and southward return flow at upper layers becomes much more extensive and vigorous, taking almost the entire ocean basin (Fig. 7f).

The weaker and shallower overturning circulation associated with the NADW production in the LGM simulation is largely supported by the observed proxy evidence (e.g., Boyle and Keigwin 1987; Rutberg et al. 2000). The reduced North Atlantic overturning circulation simulated in CGCM2 is consistent with some model results (e.g., Fichefet et al. 1994; Weaver et al. 1998), but again differs from studies based on some coupled models (Hewitt et al. 2001, 2003; Kitoh et al. 2001). This difference in the response of the North Atlantic overturning between CGCM2 and the coupled models is associated with the representation of freshwater flux to the northern North Atlantic. For example, Hewitt et al. (2003) obtained an increase in negative buoyancy flux of the surface waters across the North Atlantic and Labrador Sea and this together with extremely cold ocean conditions results in the stronger overturning at the LGM.

The CCCma coupled model appears to have the same solution of the North Atlantic overturning circulation for both the reduced and increased CO_2 concentration cases. Using the first version of CCCma coupled model

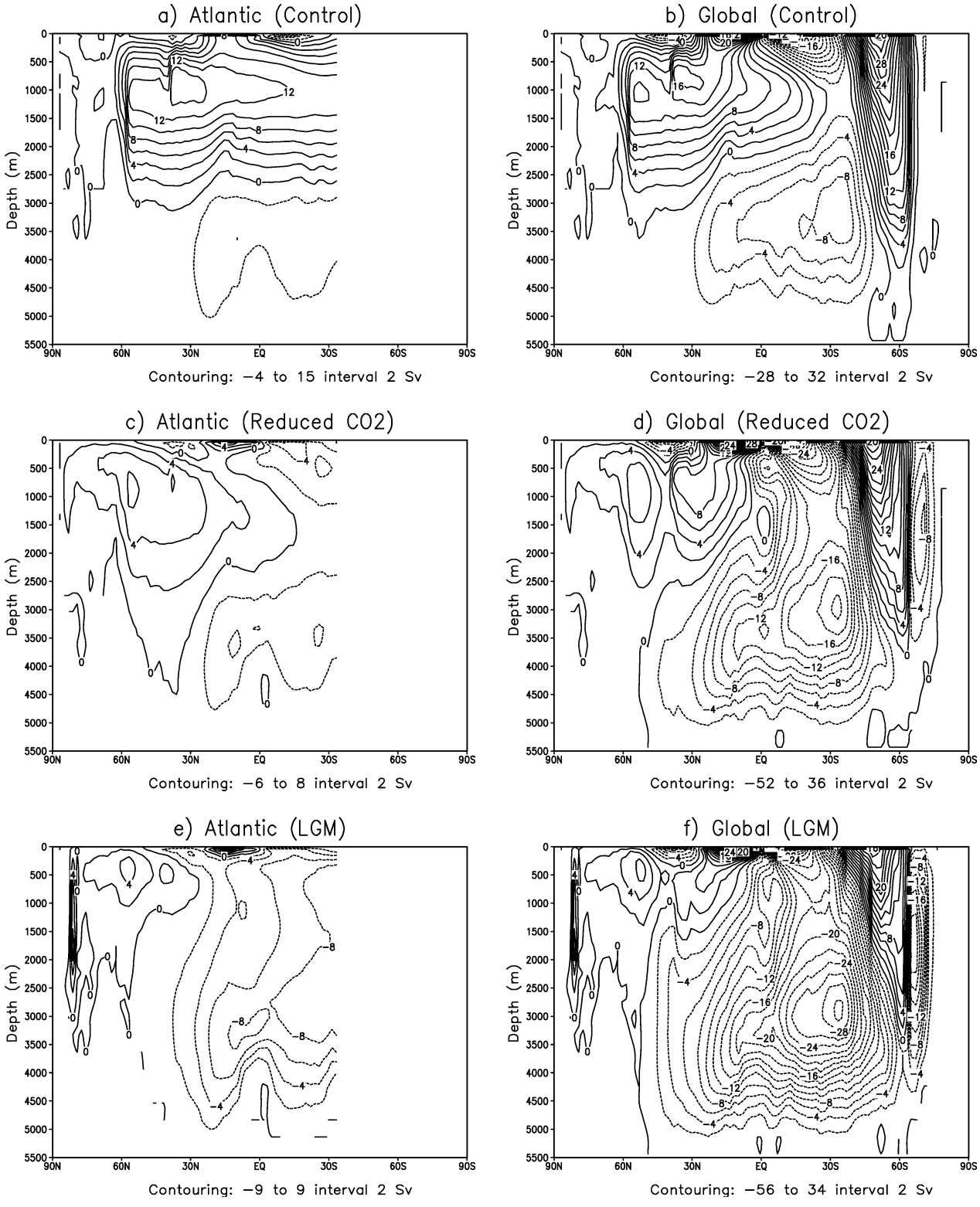

Fig. 7 Annual-mean meridional stream function for the Atlantic domain simulated in **a** control, **c** reduced CO_2, and **e** LGM, and for the global domain simulated in **b** control, **d** reduced CO_2, and **f** LGM. Units Sv ($10^6 m^3 s^{-1}$)

(CGCM1) Boer et al. (2000) obtained a reduced overturning circulation by about 60% with the doubling of greenhouse gas concentration. The weakening of overturning circulation for the decreased and increased CO_2 concentration is associated with the freshening of the northern North Atlantic (see following section), but different freshwater sources are implicated. In the case of greenhouse gas increase, the North Atlantic freshening is

mainly due to the increase in precipitation rate (Boer et al. 2000), whereas in the reduced CO_2 case it is due to the changes in net hydrological budget over the North Atlantic and river discharge as described in following section.

Overall, both the reduced CO_2 concentration and ICEAN cases result in a remarkable decrease in the overturning circulation associated with the NADW production and outflow and this change leads to a marked decrease in northward meridional heat transport. A reversed case is found in the Southern Ocean.

5.3 Surface salinity changes

The change in the overturning circulation is closely linked to the change in ocean convection and the convection is governed by the change in surface ocean density. Because the sea surface temperature decreases almost everywhere for both cases as shown in Fig. 3, the SST change should lead to an increase in surface density. This suggests that the reduction in the North Atlantic overturning circulation is due to a freshening of the surface ocean.

Figure 8 displays the geographic distribution of the change in sea surface salinity (SSS). For both cases, a marked reduction in SSS is visible in the North Atlantic.

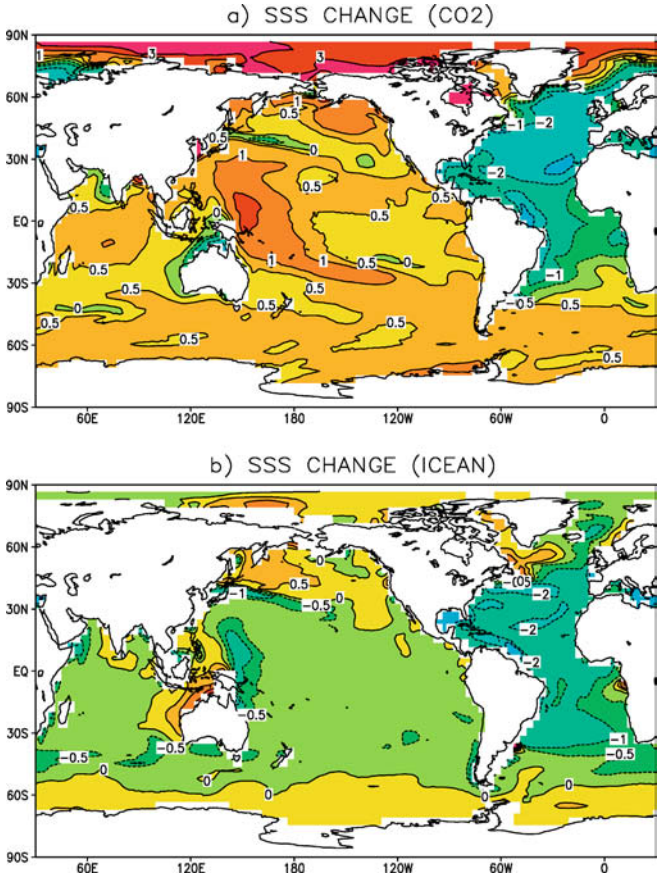

Fig. 8 Geographic distribution of the change in annual-mean sea surface salinity (SSS) for **a** CO_2 and **b** ICEAN cases. Units psu

The freshening in the North Atlantic is consistent with the reduction in the overturning circulation as described in the previous section. Analysis of the global hydrological budget change indicates that the changes in SSS broadly mirror the changes in precipitation (P) minus evapotranspiration (E) which increase in the Atlantic for both cases (not shown). In addition to the change in the hydrological budget, the large increase in river discharge in the Mississippi and Amazon rivers also plays a role in the reduction of SSS in the North Atlantic as discussed by Kim et al. (2003) in an LGM context.

Over the Southern Ocean, SSS increases substantially for the CO_2 case and slightly for the ICEAN case. This SSS increase together with the SST reduction should enhance the formation and outflow of the overturning circulation associated with AABW seen in the previous section. Another notable feature is found over the Arctic Ocean where SSS increases remarkably in the CO_2 case by more than 3 psu, while it is not evident in the ICEAN case. This marked increase is presumably associated with the increase in brine release and the arid climate over the high northern latitudes.

On the whole, the substantial reduction in SSS in the North Atlantic outweighs the slight increase in density due to the reduction of SST and the reduced density consequently results in a marked reduction in North Atlantic overturning and associated meridional heat transport. On the other hand, in the Southern Ocean both the changes in SST and SSS lead to a strengthening of the overturning circulation, taking a predominant role in deep ocean circulation.

6 Summary and conclusions

This study investigates the role of reduced atmospheric CO_2 concentration and the expanded ice-sheet topography plus associated land albedo change due to sea level drop for the maintenance of the LGM climate using a fully coupled atmosphere-ocean GCM. The model used in this study includes 3-D ocean dynamics and thermodynamics to enable meridional ocean heat transport and its role in maintaining the LGM climate.

The reduced atmospheric CO_2 concentration results in a larger cooling in global means by more than 30% for surface air temperature (SAT) and by more than 100% for sea surface temperature (SST) than that due to the ice-sheet topography plus land albedo change. The surface cooling is substantially larger in the NH than in the SH for both cases and this inter-hemispheric asymmetry is more pronounced in the ice-sheet topography case, as expected, due to the presence of the Laurentide and Fennoscandian ice sheets. The larger NH cooling exhibited in the reduced CO_2 case is consistent with the model result of HM97, but contrasts with BM87 where the CO_2-induced cooling is similar in both hemispheres or even slightly larger in the SH.

As one would expect, the surface cooling in the CO_2 case is largely due to the change in longwave heat

flux, while in the ICEAN case it is primarily due to the reduction in the shortwave heat flux because of the high reflectivity of ice. The overall reduction in the net radiative heat flux results in the surface cooling which accompanies the reduction in evaporation and results in a latent heat gain. Consequently, the reduction in radiative heat flux is largely offset by an increase in turbulent heat fluxes, but not completely due to the oceanic advective heat flux adjustment. This is particularly large in the CO_2 case.

Substantial differences in surface heat budget between CGCM2 and other models are found. For example, both BM87 and HM97 found a roughly evenly reduced radiative heat flux in both hemispheres with the reduction in CO_2 concentration, while the CGCM2 reduction is larger in the NH. In CGCM2 the snow and sea-ice albedo feedback is presumably larger than these models associated with the change in meridional ocean heat transport by the incorporation of the oceanic dynamics.

For both cases, the sea surface salinity (SSS) decreases markedly in the North Atlantic, while SSS slightly increases over the Southern Ocean. In the North Atlantic the substantial decrease in surface salinity leads to a reduction in surface density that consequently results in a substantial weakening of the overturning circulation. For example, in the reduced CO_2 simulation the NADW production decreases to 6 Sv from about 12 Sv in the control simulation, and the ICEAN leads to an additional decrease by about 2 Sv. In the Southern Ocean, the slight increase in surface salinity together with the reduced surface temperature results in an increase in surface density and consequently the overturning circulation associated with the AABW production. The deep northward AABW outflow coupled with upper ocean return flow becomes much more vigorous. The decrease (increase) in the North Atlantic (Southern Ocean) overturning circulation results in a marked reduction (enhancement) in northward (southward) ocean meridional heat transport for both cases.

In conclusion, the reduction of atmospheric CO_2 concentration accounts for about 60% of total LGM climate change, especially for the surface cooling, the change in the overturning circulation, and the ocean meridional heat transport. The rest of LGM climate change is largely accounted for by the ice-sheet topography and its associated land albedo change. Whereas the ice-sheet topography results in a large modification in the surface temperature pattern over land, the reduced CO_2 concentration appears to play an important role in shaping the spatial distribution and the magnitude of surface temperature over ocean through a larger ocean dynamic feedback.

Acknowledgements The simulations discussed in this study were made while the author was at the Canadian Centre for Climate modelling and analysis (CCCma) and this study greatly benefited from the consistent support and helpful comments by George Boer and Greg Flato. The author also wishes to thank other CCCma colleagues, especially Bernard Miville, Warren Lee, Daniel Robitaille, and Fouad Majaess for model and technical support. Valuable comments from colleagues at Duke University, especially Thomas Crowley, William Hyde, and Jesse Kenyon are appreciated. The author would like to thank to Anthony Broccoli and anonymous reviewer for their constructive reviews. This study was supported by the Climate System History and Dynamics (CSHD) program and Canadian Climate Research Network, Climate Variability Project.

References

Barnola JM, Raynaud D, Korotkevich YS, Lorius C (1987) Vostok ice core provides 160 000-year record of atmospheric CO_2. Nature 329: 408–418

Boer GJ (1993) Climate change and the regulation of the surface moisture and energy budget. Clim Dyn 8: 225–239

Boer GJ, Yu B (2003) Climate sensitivity and response. Clim Dyn 20: 415–429

Boer GJ, McFarlane NA, Lazare M (1992) Greenhouse gas-induced climate change simulated with the CCC second-generation general circulation model. J Clim 5: 1045–1077

Boer GJ, Flato GM, Ramsden D (2000) A transient climate change simulation with greenhouse gas and aerosol forcing: projected climate to the twenty-first century. Clim Dyn 16: 427–450

Boyle EA, Keigwin L (1987) North Atlantic thermohaline circulation during the past 20 000 years linked to high-latitude surface temperature. Nature 330: 35–40

Broccoli AJ (2000) Tropical cooling at the Last Glacial Maximum: an atmosphere-mixed layer ocean model simulation. J Clim 13: 951–976

Broccoli AJ, Manabe S (1987) The influence of continental ice, atmospheric CO_2, and land albedo on the climate of the last glacial maximum. Clim Dyn 1: 87–99

Broecker WS, Henderson GM (1998) The sequence of events surrounding Termination II and their implications for the cause of glacial-interglacial CO_2 changes. Paleoceanogr 13: 352–364

CLIMAP (1976) The surface of the Ice-Age Earth. Science 191: 1131–1136

CLIMAP (1981) Seasonal reconstructions of the Earth's surface at the last glacial maximum. Geol Soc Am Map Chart Ser, MC-36

Crowley TJ, Baum SK (1997) Effect of vegetation on an ice-age climate model simulation. J Geophys Res 102: 16463–16480

Fairbanks RG (1989) A 17000-year glacio-eustatic sea level record: influence of glacial melting rates on the Younger Dryas event and deep-ocean circulation. Nature 342: 637–642

Fichefet T, Hovine A, Dupplessy J-C (1994) A model study of the Atlantic thermohaline circulation during the last glacial maximum. Nature 372: 252–255

Flato GM, Hibler III WD (1992) Modelling pack ice as a cavitating fluid. J Phys Oceanogr 22: 626–651

Flato GM, Boer GJ (2001) Warming asymmetry in climate change simulations. Geophys Res Lett 28: 195–198

Flato GM, Boer GJ, Lee WG, McFarlane NA, Ramsden D, Reader MC, Weaver AJ (2000) The Canadian Centre Climate Modelling and Analysis global coupled model and its climate. Clim Dyn 16: 451–467

Ganachaud A, Wunsch C (2000) Improved estimates of global ocean circulation, heat transport and mixing from hydrographic data. Nature 408: 453–457

Ganopolski A, Rahmstorf S, Petoukhov V, Claussen M (1998) Simulation of modern and glacial climates with a coupled global model of intermediate complexity. Nature 391: 351–356

Gent PR, McWilliams JC (1990) Isopycnal mixing in ocean circulation models. J Phys Ocenaogr 20: 150–155

Genthon C, Barnola JM, Raynaud D, Lorius C, Jouzel J, Barkov NI, Korotkevich YS, Kotlyakov VM (1987) Vostik ice core: climatic response to CO_2 and orbital forcing changes over the last climatic cycle. Nature 329: 414–418

Hansen J, Lacis A, Rind D, Russell G, Stone P, Fung I, Ruedy R, Lerner J (1984) Climate sensitivity: analysis of feedback mechanisms. In: Hansen J, Takahashi T (eds) Climate processes and climate sensitivity. Geophys Mono 29, Am Geophys Union, Washington, DC, 130–163

Hansen J, Lacis A, Ruedy R, Sato M, Wilson H (1993) How sensitive is the world's climate? Nat Geogr Res Explor 9: 143–158

Hansen J, Sato M, Ruedy R (1997) Radiative forcing and climate response. J Geophys Res 102: 6831–6864

Hays JD, Imbrie J, Shackleton NJ (1976) Variations in the Earth's orbit: pacemaker of the ice ages. Science 194: 1121–1132

Haywood JM, Stouffer RJ, Wetherald RT, Manabe S, Ramaswamy V (1997) Transient response of a coupled model to estimated changes in greenhouse gas and sulfate concentrations. Geophys Res Lett 24: 1335–1338

Hewitt CD, Mitchell JF (1997) Radiative forcing and response of a GCM to ice age boundary conditions: cloud feedback and climate sensitivity. Clim Dyn 13: 821–834

Hewitt CD, Broccoli AJ, Mitchell JF, Stouffer RJ (2001) A coupled model study of the last glacial maximum: was part of the North Atlantic relatively warm? Geophys Res Lett 28: 1571–1574

Hewitt CD, Stouffer RJ, Broccoli AJ, Mitchell JF, Valdes PJ (2003) The effect of ocean dynamics in a coupled GCM simulation of the Last Glacial Maximum. Clim Dyn 20: 203–218

Hoffert MI, Covey C (1992) Deriving global climate sensitivity from paleoclimate reconstructions. Nature 360: 573–576

Imbrie J, Hays JD, Martinson DG, McIntyre A, Mix AC, Morley JJ, Pisias NG, Prell WL, Shackleton NJ (1984) The orbital theory of Pleistocene climate: Support from a revised chronology of the marine ^{18}O record. In: Berger AL et al. (eds) Milankovitch and Climate, Part 1. Dordrecht, Netherlands, pp 269–305

Jouzel J, Lorius C, Petit JR, Genthon C, Barkov NI, Kotlyakov VM, Petrov VM (1987) Vostok ice cores: a continuous isotope temperature record over the last climatic cycle (160 000 years). Nature 329: 403–408

Kim S-J, Flato GM, Boer GJ, McFarlane NA (2002) A coupled climate model simulation of the Last Glacial Maximum, Part 1: transient multi-decadal response. Clim Dyn 19: 515–537

Kim S-J, Flato GM, Boer GJ, McFarlane NA (2003) A coupled climate model simulation of the Last Glacial Maximum, Part 2: approach to equilibrium. Clim Dyn 20: 635–661

Kitoh A, Murakami S, Koide H (2001) A simulation of the Last Glacial Maximum with a coupled atmosphere-ocean GCM. Geophys Res Lett 28: 2221–2224

Manabe S, Broccoli AJ (1985) The influence of continental ice sheets on the climate of an ice age. J Geophys Res 90: 2167–2190

Manabe S, Stouffer RJ, Spelman MJ, Bryan K (1991) Transient responses of a coupled ocean-atmosphere model to gradual changes of atmospheric CO_2. Part I: annual mean response. J Clim 4: 785–818

Macdonald AM, Wunsch C (1996) An estimate of global ocean circulation and heat fluxes. Nature 382: 436–439

McFarlane NA, Boer GJ, Blanchet J-P, Lazare M (1992) The Canadian Climate Centre second-generation general circulation model and its equilibrium climate. J Clim 5(10): 1013–1044

Milankovitch M (1941) Canon of insolation and the ice age problem. K Ser Aka, Beograd (English translation by the Israel Program for the Scientific Translation). Special Publ 132, US Department of Commerce and Natl Sci Fdn, Washington, DC, USA

Neftel A, Oeschger H, Schwander J, Zumbrunn R (1982) Ice core sample measurements give atmospheric CO_2 content during the past 40,000 years. Nature 295: 200–223

Peltier WR (1994) Ice age paleotopography. Science 265: 195–201

Ramaswamy V, Chen C-T (1997) Linear additivity of climate response co combined albedo and greenhouse perturbations. Geophys Res Lett 24: 567–570

Rutberg RL, Hemming SR, Goldstein SL (2000) Reduced North Atlantic deep water flux to the glacial Southern Ocean inferred from neodymium isotope ratios. Nature 405: 935–938

Semtner AJ (1976) A model for thermodynamic growth of sea ice in numerical investigations of climate. J Phys Oceanogr 6: 379–389

Shin S-I, Liu Z, Otto-Bliesner B, Brady E, Kutzbach J, Harrison S (2003) A simulation of the Last Glacial Maximum climate using the NCAR-CCSM. Clim Dyn 20: 127–151

Stouffer RJ, Manabe S (1999) Response of a coupled ocean-atmosphere model to increasing atmospheric carbon dioxide: Sensitivity to the rate of increase. J Clim 12: 2224–2237

Voss R, Sausen R (1996) Techniques for asynchronous and periodically-synchronous coupling of atmosphere and ocean models, Part II: impact of variability. Clim Dyn 12: 605–614

Weaver AJ, Eby M, Fanning AF, Wiebe EC (1998) Simulated influence of carbon dioxide, oribital forcing and ice sheets on the climate of the last glacial maximum. Nature 394: 847–853

Wyputta U, McAvaney BJ (2001) Influence of vegetation changes during the Last Glacial Maximum using the BMRC atmospheric general circulation model. Clim Dyn 17: 923–932